Talanta 220 (2020) 121303

Contents lists available at ScienceDirect

Talanta

journal homepage: www.elsevier.com/locate/talanta

Video colorimetry of single-chromophore systems based on vector analysis in the 3D color space: Unexpected hysteresis loops in oscillating chemical reactions

Joseph Schell [a,b], Sara C. McCauley [a], Rainer Glaser [a,*]

[a] Department of Chemistry, Missouri University of Science and Technology, Rolla, MO, 65409, USA
[b] Department of Chemistry, University of Missouri, Columbia, MO, 65211, USA

ARTICLE INFO

Keywords:
Colorimetry
RGB Color space
Vector projection
Belousov-Zhabotinsky oscillating reaction
Video-based kinetics
Hysteresis loops

ABSTRACT

Colorimetry, the quantitative determination of color, usually of a digital image, has useful applications in diverse areas of research. Many methods have been proposed for translating the RGB data of an image to obtain concentration information. Among the many methods for RGB analysis, we focus on the vector projection method (VP), which is based on a vector analysis in 3D RGB color space. This method has the major advantages of being conceptually intelligible and generalizable to various systems. For solutions with variable concentrations of one chromophore, we will show that the analysis of the trace in RGB color space allows for a judgment about the reliability of the linear concentration dependence of the chromapostasi parameter. We discuss the theoretical underpinnings of the method in two test cases, a simple dye solution and a titration of an organic acid with phenolphthalein indicator. The VP method was then applied to the Ce-catalyzed Belousov-Zhabotinsky reaction with the expectation that the colorimetry would quantify [Ce^{4+}] oscillations. Surprisingly, the 3D color space analysis revealed hysteresis loops and the origin and implications of this observation are discussed.

1. Introduction

Colorimetry is a technique that allows for the determination of the concentration of an analyte based on the color information of a given image. Most often, images are taken with a digital camera, and the pixel information is translated to intensities of red, green, and blue (RGB) light, on a scale that ranges from 0 to 255 for each color. The mixture of the RGB primary colors controls the overall color perceived by the user (Fig. S1). Black is perceived when all three intensities are zero and white is perceived when all three intensity values are 255. Colorimetry has been gathering increasing interest in recent years, especially with the development of smartphone cameras [1–3]. The multitude of useful applications has launched a wave of innovation within colorimetry to enhance standard analytical techniques [4–6] and inform emerging neural-networking applications [7]. The range of specialized applications includes the detection of explosives [8], food additives [9,10], drugs [11,12], and various trace metals in aqueous solutions [13,14]. Exciting biomedical applications include protein detection and discrimination [1], diagnosis of drug resistant diseases [15], and the monitoring of cell culture viability [16].

Colorimetry intrinsically seeks to quantify concentration and it is desirable to have a physically meaningful, reliable *process* (i.e., the treatment of the RGB values) that is generalizable to all colorimetric studies. In practice, many different combinations of the R, G, and B intensity data have been shown empirically to have strong correlations with concentration, and different treatments have been more or less effective for different datasets [17,18]. An excellent comparison of various RGB-derived parameters is given in Table 1 of Ref. 8 in which Choodum et al. [8] explored various combinations of RGB data and many parameters showed strong correlation with concentration. Lopez-Molinero et al. [13] compared some of the more popular treatments and also found concentration to strongly correlate with several RGB-derived parameters. Dong et al. [19] and Lyra et al. [5] explored a vector analysis approach, which relies on the Euclidean distance in color space between the sample and a reference. It is an appealing aspect of this approach that it has clear theoretical underpinnings. We will develop this basic approach for our purposes (*vide infra*).

The Belousov-Zhabotinsky oscillating chemical reactions (BZR) is a prototypical example of nonlinear dynamics [20–22]. The unstirred BZ reaction features intriguing wave propagations in real space which have

* Corresponding author.
E-mail address: GlaserR@mst.edu (R. Glaser).

https://doi.org/10.1016/j.talanta.2020.121303
Received 21 May 2020; Received in revised form 15 June 2020; Accepted 16 June 2020
Available online 11 July 2020

been studied colorimetrically [23–25]. Our group has been interested in studying mechanistic aspects of the bromine chemistry [26,27] and measuring the kinetics of the stirred BZ reaction using video colorimetry methods [28,29]. To determine the oxidation and reduction times using colorimetry, we employed the "Difference from Characteristic Color" (DCC) approach, a root-mean-square-deviation based analysis (*vide infra*), and we have shown this DCC approach to work very well [28,29]. In our previous studies, it was assumed that the DCC intensities would correlate with the concentration of the metal catalyst in solution. To test this assumption, we are examining here several case studies both with colorimetric methods and independent concentration measures. In the process, we developed a refined DCC method, the DCC_{ED} method, and we compared the performance of both DCC methods to the results obtained with an RGB vector-based analysis. The Vector Projection (VP) approach compares the measured RGB data of the sample to the color of a blank solution in RGB color space. With the VP approach we are able to determine the concentration of a single chromophore in dilute solution with high accuracy and reliability. As a proof of concept, we compared these colorimetric methods to UV–Vis data in a study of the concentration dependence of a simple dye solution and to theoretically calculated concentrations of phenolphthalein indicator over the course of a titration. With the reliability of the VP method demonstrated in this way, we applied it to successfully determine the concentration of Ce^{4+} in a cerium-catalyzed BZR. Colorimetry of a series of solutions with Ce^{4+} concentrations in the range of the BZ reaction shows the expected linear trace in 3D RGB space. The buildup of Ce(IV) during the fast oxidation phase of a BZR cycle initially follows a linear trace as expected. Surprisingly, however, this linearity does not persist for the entire oxidation phase and a different and complicated path is traced in the slow reduction phase. The hysteresis loops show shape-stability across BZR cycles and the origin and implications of this observation are discussed.

2. Methods

2.1. Instrumentation and setup

For the color analyses, it is important to be as consistent as possible with the background and lighting features [30]. To this end, we used a white poster board as a background for each video/set of images. We used room lighting in conjunction with one or two photography lights to increase the overall light intensity. The white balance function of the camera was also used, and was adjusted, either automatically or manually, at the beginning of each dataset. Care was taken to place the camera at the beginning of each run in a given position such that the image of the reaction vessel was clear. The approximate distance from the camera to the beaker was 34 cm. Once the camera was placed, it was not moved for the duration of the data collection. Consistency in these aspects within any dataset is essential to obtaining good data; consistency across datasets is generally desirable, but less important.

UV spectra were recorded on an Agilent Cary 60 UV–Visible spectrophotometer with a Xenon flash lamp. The fiber optic dip probe accessory was used to collect data in real time. Scans were collected at a moderate scan rate over a small range of wavelengths in the region of absorbance.

2.2. Data extraction from video/images

2.2.1. Video recording and image collection

Videos and images were recorded with a Panasonic HC-V110 8.9 megapixel camera, which can capture video in three different formats, AVCHD, iFrame, and MP4. In this study, we used the maximum resolution of the camera, 1080p for video (AVCHD) and 3968x2232 for still images. The analysis includes selecting a small window of each image that contains a set number of pixels (*vide infra*). A higher resolution also affords the option to use much larger sample windows, should that be desired. The capture rate of the camera for videos was 29 frames per second (fps). AoAo software [31,32] was used to convert the videos into a series of still images without quality loss and during this conversion, the image rate was set to 10 images per second to reduce the number of files and therefore the analysis time. The effect of frame rate and sample window size on analysis time was studied previously [28]. For some kinetics applications, a higher frame rate would be desirable.

2.2.2. Placement and size of sample window

After generating the images that will be analyzed, some small window of pixels must be defined that will be used in the analysis. In this study, we use either a 50x50 pixel or a 100x100 pixel sample window. The placement of the window was dictated by several factors. In the BZ reaction vessel, we often add stirring elements and/or measurement probes to the beaker which obstruct the view of solution. Stirring effects (e.g., vortex from fast stirring) and reflections on the glassware from external lighting are also key features to avoid. Finally, in the BZR, CO_2 is produced over the course of reaction, giving rise to bubbles that can adhere to the walls of the glass. The sample window chosen should be relatively clear of bubbles, even in the later portions of the video when the most bubbles are present in solution. We define a sample window that is as far removed as possible from these elements to achieve an accurate estimate of the solution color (Fig. S2).

It should be noted that the choice of sample window also affects the path length through the solution. Even within a sample window, points on opposite sides of the grid have slightly different path lengths due to the cylindrical shape of the reaction vessel. To determine whether these differences would have any effect on the results, we analyzed a single dataset several times with different window placements. We found no measurable deviation in the average solution color and therefore find the effect of these small path length differences to be negligible.

2.2.3. Reference and blank solutions

The determination of concentration via any colorimetric method requires at least one reference solution of known concentration. The concentrations of samples can then be determined by extrapolation, within reasonable limits (i.e., dilute solutions). For the simple systems described here that start colorless and acquire color over time, the reference solution will be a single-component solution of the analyte. It is well known that the absorbance of a solution follows Beer's Law, that is, the absorbance is directly proportional to concentration for dilute solutions [33]. Therefore, reference solutions should be relatively lightly colored such that their concentrations are in the range of concentrations where Beer's Law holds. In the discussion of the study of the dye solution with our colorimetric methods, we will show at which concentrations Beer's Law begins to fail. Knowing this critical concentration, we can verify that the reference solution chosen falls within the range of proportionality.

One primary difference between the vector projection method and the DCC methods outlined below is the choice of reference solution (Scheme 1). For ideal results with the DCC methods, the reference solution will have the maximum concentration for which Beer's Law still holds. This is because the DCC methods calculate the concentration of a species based on the difference between the RGB intensities of the sample point and the reference point (*vide infra*) and the *direction* of color change from the reference is not included in the calculation. Therefore, the reference should be as deeply colored as possible within the limit of Beer's Law, such that images that deviate from the characteristic color can be assumed to be less colored and, therefore, correspond to less concentrated solutions. In Scheme 1, the region where Beer's Law applies is shown in green. The point C is the critical point where the linear relationship of the DCC value to the concentration breaks down and, therefore, point C is the ideal reference point for DCC measurements. Point B can also be used effectively, especially if all of the measured samples are less concentrated than solution B. However, the choice of point D as a standard is poor and results will be *correlated* with concentration but the correlation *will not* be linear. It is often

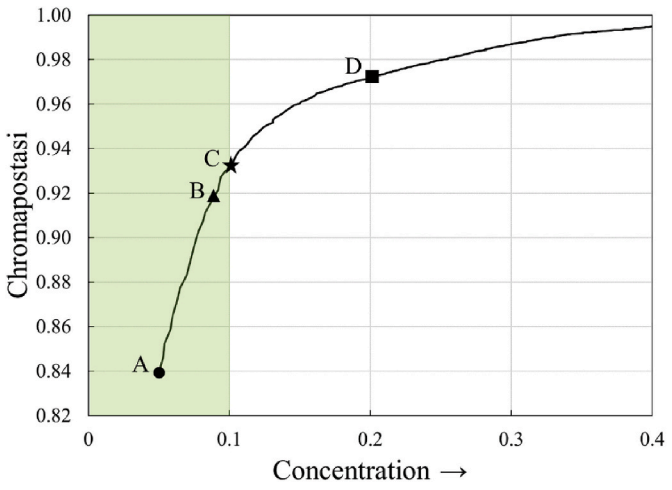

Scheme 1. Hypothetical Results of the DCC Method Highlighting Key Points to Consider as the Reference Solution.

impossible to determine critical concentration before an experimental run, and therefore the most deeply-colored solution is used as the DCC reference image and a check is performed afterwards to ensure that the concentration of the reference image lies within the allowable range.

Aside from a reference solution, the vector projection method also makes use of a blank solution. To ensure lighting conditions and other parameters are the same for the blank and the sample solutions, the blank images are usually taken immediately preceding the experimental trial. For our experiments, the blank image will contain the reaction vessel and either a water solution or a solution of the reaction mixture before any of the colored analyte is added. For example, the blank image for a BZR experiment was the mixture of the bromate, bromide, malonic acid, and sulfuric acid solutions before the Ce catalyst was added. It is preferred that the components of the blank solution be as similar to the sample matrix as possible.

2.3. Measurement of RGB values

For each sample image, the RGB values are extracted via a simple Mathematica program using the built-in ImageData function [34]. This gives an [m × n × 3] three-dimensional array of the red, green, and blue color values for each pixel for a given image (Fig. S3).

Then, we average over the red values, the green values, and the blue values of the pixels to get composite RGB values for each image (i) of the sample (Eqs. (1)–(3)).

$$R_{s.i} = \frac{\sum_1^m \sum_1^n R_{m,n}}{m * n} \tag{1}$$

$$G_{s.i} = \frac{\sum_1^m \sum_1^n G_{m,n}}{m * n} \tag{2}$$

$$B_{s.i} = \frac{\sum_1^m \sum_1^n B_{m,n}}{m * n} \tag{3}$$

These composite values correspond to a single point ($R_{s,i}$, $G_{s,i}$, $B_{s,i}$) in the RGB color space. The pixels in the blank and reference images are averaged in the same way to obtain the composite R_b, G_b, B_b and R_r, G_r, and B_r values, respectively.

2.4. DCC_0 and DCC_{ED} methods

Conceptually, the DCC analysis measures the difference between the color of a given sample and a reference image. Therefore, the DCC analysis relies both on the (R_s, G_s, B_s) points of the sample and the reference point (R_r, G_r, B_r). The DCC method is applied here in two ways, to determine the original DCC_0 values and a second set of DCC_{ED} values.

The equation for the determination of the originally described DCC_0 values [28,29] is shown in Eq. (4).

$$DCC_{0.i}(R_{s.i}, G_{s.i}, B_{s.i}) = 1 - \left(\frac{R_{s,i} - R_r}{255}\right)^2 + \left(\frac{G_{s,i} - G_r}{255}\right)^2 + \left(\frac{B_{s,i} - B_r}{255}\right)^2 \tag{4}$$

The division by 255 ensures that each of the terms is less than one and the squaring ensures that each term is positive.

In the process of working on the current project, we realized that the DCC approach could be made more physically meaningful. Specifically, we define the new parameter DCC_{ED} via Eq. (5).

$$DCC_{ED.i}(R_{s.i}, G_{s.i}, B_{s.i}) = 1 - \frac{1}{\sqrt{3}}\sqrt{\left(\frac{R_{s,i} - R_r}{255}\right)^2 + \left(\frac{G_{s,i} - G_r}{255}\right)^2 + \left(\frac{B_{s,i} - B_r}{255}\right)^2} \tag{5}$$

By taking the square root of the three summed terms in Eq. (4), the new chromapostasi function DCC_{ED} now reflects the Euclidean distance in color space between the reference image and the sample image (Eq. (5)). The term "chromapostasi" reflects that DCC_{ED} is a measure of the distance (Greek, apostasi) between points in color (Greek, chroma) space.

We emphasized above the importance of using a reference solution with a concentration at the upper end of the experimental range of interest. With Eqs. (4) and (5) the reason for this condition becomes clear: the DCC value will increase with increasing concentration until the concentration of the sample matches that of the reference solution. However, for samples with higher concentrations than the reference solution, whether within the Beer's Law range or not, DCC will decrease. For the case studies presented in the following, it is always the case that the concentrations of the DCC reference solutions exceed the concentration range of the sample solutions.

2.5. Vector projection

The vector projection method relies on the difference vectors $\vec{A}$ which are defined with Eq. (6) by the difference between the sample ($R_{s,i}$, $G_{s,i}$, $B_{s,i}$) point and the blank point (R_b, G_b, B_b). A difference vector $\vec{B}$ is defined for the reference image as shown in Eq. (7).

$$\vec{A_i} = (R_{s,i}, B_{s,i}, G_{s,i}) - (R_b, G_b, B_b) \tag{6}$$

$$\vec{B} = (R_r, B_r, G_r) - (R_b, G_b, B_b) \tag{7}$$

$$\vec{A_i} = \sqrt{(R_{s,i} - R_b)^2 + (G_{s,i} - G_b)^2 + (B_{s,i} - B_b)^2} \tag{8}$$

$$\vec{B} = \sqrt{(R_r - R_b)^2 + (G_r - G_b)^2 + (B_r - B_b)^2} \tag{9}$$

The magnitudes of vectors $\vec{A}$ and $\vec{B}$ are given by Eqs. (8) and (9), respectively. We will show that these magnitudes are directly proportional to concentration over a given range. Thus, by comparing the magnitude $\vec{A_i}$ of the i^{th} sample image to that of the reference solution $\vec{B}$, we can estimate to a very good approximation the concentration of the sample using Eq. (10).

$$[A]_i = \frac{||\vec{A_i}||}{||\vec{B}||}[B] \tag{10}$$

In an ideal Beer's Law scenario, the trace of the $\vec{A_i}$ vectors define a straight line in color space and fall along the same line as the $\vec{B}$ vector. In reality, the $\vec{A_i}$ vectors may deviate somewhat from the direction of the $\vec{B}$ vector. In those cases, the sample vectors would need to be projected

onto the $\vec{B}$ standard vector to estimate the concentration. The vector projected magnitude (VPM) of vector $\vec{A_i}$ is provided by Eq. (11), where θ_i is the angle between each sample vector $\vec{A_i}$ and the reference vector $\vec{B}$. The angle θ_i can be determined by Eq. (12). Small θ values indicate that the vectors are directionally similar and therefore that the sample is a different shade of the same color as the reference solution.

$$VPM_i = \overrightarrow{A_i} \cos\theta_i \tag{11}$$

$$\cos\theta = \frac{\vec{A} \cdot \vec{B}}{||\vec{A}||\,||\vec{B}||} \tag{12}$$

The θ parameter becomes important in multi-chromophore systems. In a reaction that is accompanied by the transition from one color to another color, one would define two $\vec{B}$ vectors relative to the two reference colors. The associated $\theta_{1,i}$ and $\theta_{2,i}$ inform about the transition region.

In this work, we study single-chromophore solutions and, hence, the θ values are typically very small and not reported. Note that θ may get very large when the sample vectors have almost no magnitude and in these low-concentration cases θ merely reflects a signal:noise ratio error. Of course, when $\theta_i \approx 0$, VPM_i is approximated by $\vec{A_i}$ and for the cases reported here, we refer to VPM_i simply as the chromapostasi magnitude of the VP method.

3. Results and discussion

3.1. Concentration of a single colored dye solute

As a proof of concept, we analyzed a series of solutions of a simple food dye. Green food dye is a mixture of FD&C Yellow 5 (tartrazine) and Blue 1 (Brilliant Blue FCF) dissolved in water/propylene glycol. Small aliquots of the dye solution were added to a beaker containing 750 mL of water. After the addition of each aliquot, a picture of the solution was recorded with the camera and a UV–Visible spectrum was recorded in the 620–635 nm region. Dye was added until the color of the solution became dark green.

The endpoints of each sample vector (R_s, G_s, B_s) are plotted in the first panel of Fig. 1 in the 3D RGB color space as a function of dye concentration. The bottom panel of Fig. 1 shows the decomposition of the color space points into their $R_s(c)$, $G_s(c)$, and $B_s(c)$ values as a function of the dye concentration. Note that the blank solution has the *highest* R, G, and B values and that the addition of dye *decreases* the R_s, G_s, and B_s values until all three approach zero. The appearance of "more green" solution is the result of diminished intensity in the red and blue channels. In addition, Fig. 1 demonstrates in a compelling fashion that the intensity changes in the three color channels are not traceable. For example, the first 54 drops of green food dye deplete entirely the intensity of red color in an almost linear fashion. The blue values also decrease relatively quickly, but not linearly, and remain non-zero over

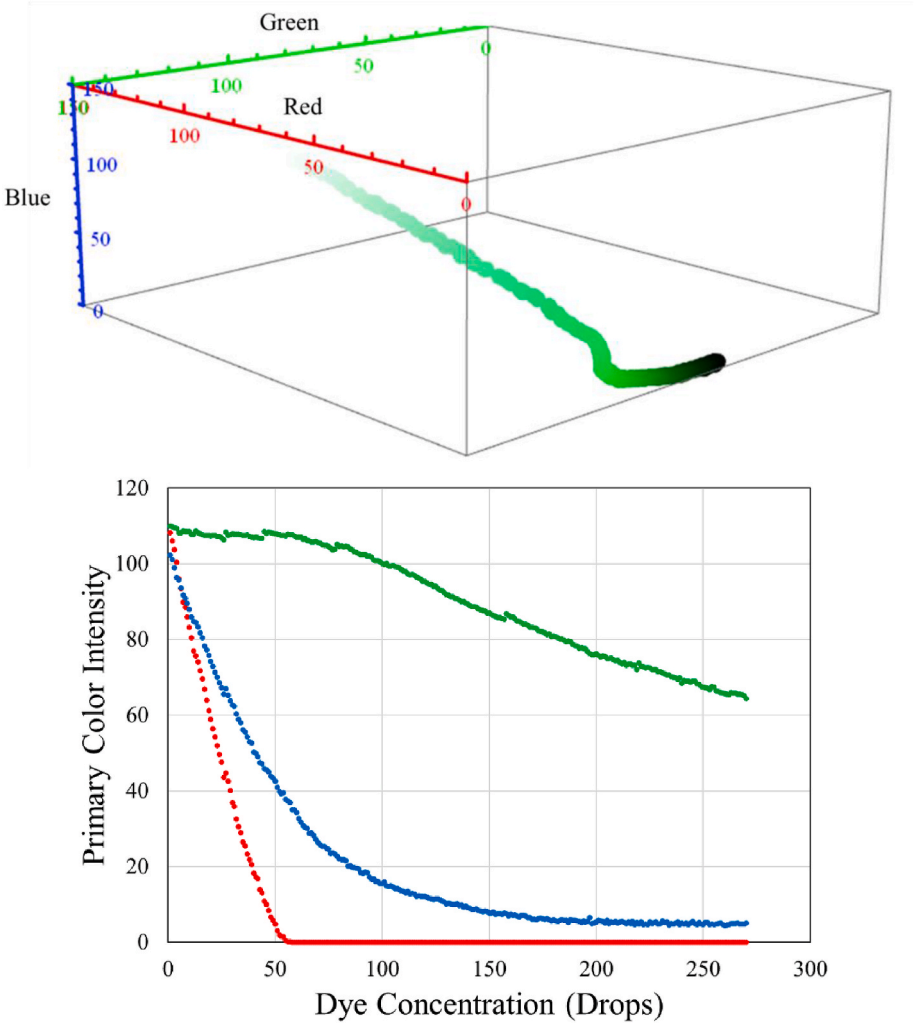

Fig. 1. Full concentration profile of green food dye in the RGB color space. Every point in the top panel corresponds to one specific concentration of the dye and each point is drawn with the color of that solution. The bottom panel shows the $R_s(c)$, $G_s(c)$, and $B_s(c)$ values with increasing concentration.

the range studied. Initially, the green values remain nearly constant and begin to decrease only after the R and B intensities are well below 20.

The UV–Vis absorbance at 630 nm was measured over the entire concentration range and the measured data are shown in Fig. S4. The UV–Vis data follow Beer's Law perfectly over the entire range of dye concentrations. To evaluate whether the video analysis can produce quantitative concentration data, we plotted the chromapostasi VPM values on the primary axis as a function of the measured absorbances over the entire range (Fig. 2, top panel, dark blue). In Fig. 2, we also show the chromapostasi values DCC_0 (dark teal) and DCC_{ED} (orange) plotted on the secondary axis.

The plot in Fig. 2 shows that the VPM chromapostasi values can reflect analyte concentration, but it also shows that the linear relation between $\overrightarrow{A_i}$ values and absorbances for this dataset is limited to concentrations below an absorbance of 0.14. The bottom panel shows a close-up of the region in which the chromapostasi values correlate linearly with measured absorbances.

The insights of Fig. 1 combined with the observation of Fig. 2 suggest that chromapostasi measurements can reflect concentration changes only if the intensities in *all* channels remain above a certain threshold. In our specific case, the R intensity becomes zero after the addition of 54 drops of dye solution and for higher dye concentrations the VP method no longer tracks concentration linearly. This observation explains why some previous studies found analyses of only one color channel to sometimes be just as effective as measuring all three color channels [8].

The bottom panel in Fig. 2 shows that the VPM values correlate with absorbances below 0.14 (dotted line) in a linear fashion with $R^2 > 0.98$. Further reduction of the upper absorbance limit to 0.1 results in an even better linear fit with $R^2 > 0.99$ (dashed line). All three methods show somewhat linear correlation up to a certain point, and then deviate from linearity at high concentrations. The DCC_0 and DCC_{ED} values correlate with concentration and the DCC_{ED} values are better compared to the DCC_0 data.

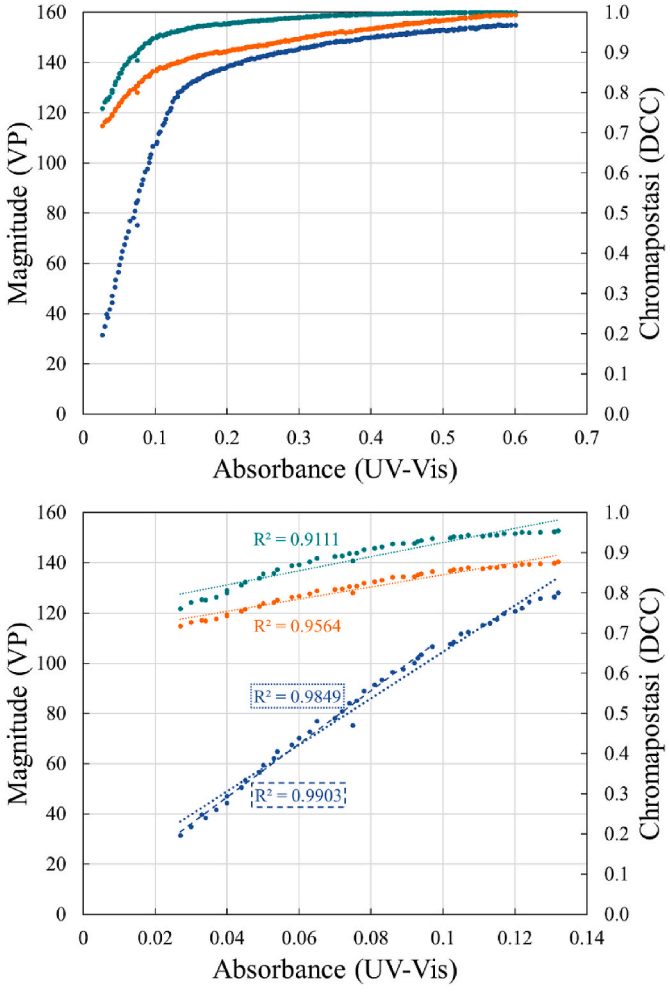

Fig. 2. Comparison of the Vector Projection method (Dark Blue) and the DCC methods, DCC_0 (Dark Teal) and DCC_{ED} (Orange) to UV–Vis data.

The above discussion has one immediate consequence, namely that the selection of a shorter path length should increase the linear range of the video analysis. To make this point, the green dye experiment was performed again measuring the UV–Vis absorbance and video data in a standard quartz cuvette (1 cm path). The top portion of Fig. S5 shows the R_s, G_s, and B_s values for each concentration of dye solution measured in the cuvette, analogous to the bottom panel of Fig. 1. Similarly, the bottom panel of Fig. S5 shows the results of the VP analysis as a function of the UV–Vis absorbance, analogous to Fig. 2. Fig. S5 illustrates in a compelling fashion that the shortened path length drastically increases the concentration range in which the video analysis produces chromapostasi data that linearly correlate with concentration. With the small path length, we find an excellent linear correlation between the UV–Vis absorbances and the video data ($R^2 = 0.9953$) for the region from 0 to 1.0 absorbance, a ten-fold increase!

3.2. Titration of acetic acid with phenolphthalein indicator

The study of the pH titration of acetic acid is more challenging than the study of the simple dye solutions for two reasons. First, the color change in a titration occurs rapidly in a small region of the entire pH range. Second, the concentration of the colored analyte is less clear because it exists in equilibrium with other species, and therefore, its concentration must be determined by an independent method.

Fig. 3 shows the individual R_s, G_s, and B_s values as a function of the volume of base added. This is analogous to Fig. 1 for the dye. The color change of phenolphthalein from colorless to pink begins around 36.9 mL of base added. Note that the *increase* of pink color is reflected by a sharp *decrease* in the green channel, the complementary color. The pink of the phenolphthalein dianion is a mixed color of red and blue with red dominating ("reddish pink"). Accordingly, we observe a faster *decrease* in the blue channel as compared to the red channel with increasing chromophore concentration. Note that none of the primary color intensities dips below 20 and all three values continue to decrease with increasing $[In^{2-}]$ for the entire course of the titration. The corresponding change in color space traces out an approximately straight line.

In Fig. 4, we plot the results of the colorimetric analysis as a function of volume of base added. The top panel shows the results of the VP method and the bottom panel shows the results of the DCC methods. In both panels of Fig. 4, we show the concentrations of the colored analyte on the secondary axis. The main purpose of our paper is the demonstration of video-based colorimetric analysis following species concentrations. In the case of the green dye study, we employed UV–Vis spectroscopy and Beer's Law to obtain reliable concentration information. Here, we provide reliable concentration information about the chromophore in a different way, namely via simulation of the multi-equilibrium system as a function of pH [35–37].

Phenolphthalein is a neutral acid, H_2In, at low pH values and the loss of two protons affords a pink dianion species, In^{2-}. The overall reaction is shown below as R1 and the equilibrium constant expression is given by Eq. (13). Of course, this reaction can be split into single proton dissociation reactions R1a and R1b with the associated equilibrium constant expressions of Eq. (14) and Eq. (15).

$$H_2In \rightleftharpoons 2\,H^+ + In^{2-} \quad \text{(R1)}$$

$$K_{eq} = [H^+]^2\,[In^{2-}] \,/\, [H_2In] \quad (13)$$

$$H_2In \rightleftharpoons H^+ + HIn^- \quad \text{(R1a)}$$

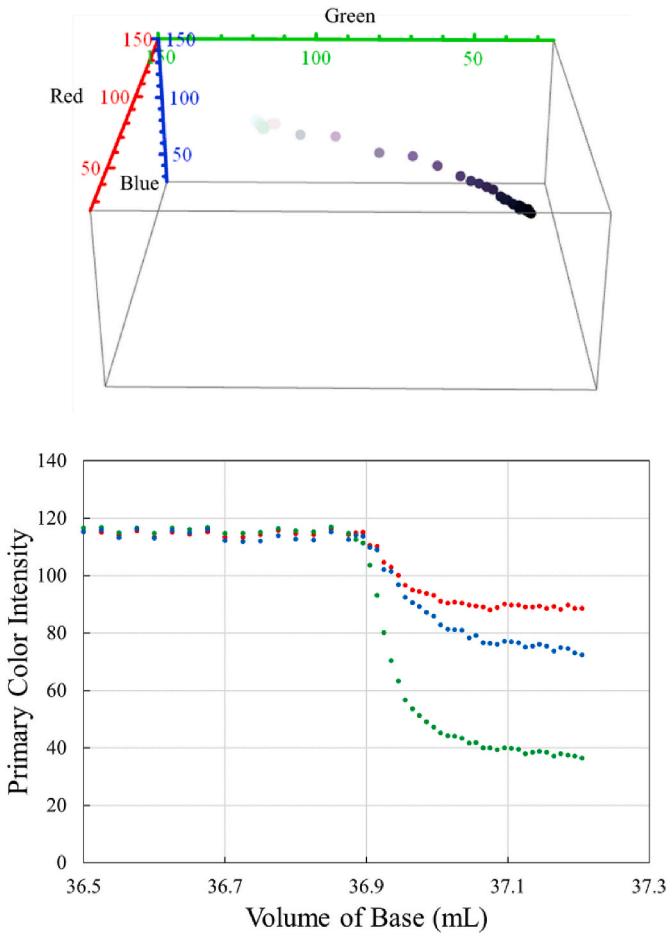

Fig. 3. Composite R_s, G_s, and B_s values as a function of base added shown in the 3D color space (top) and as the individual primary color intensities (bottom). The color change of phenolphthalein starts at around 36.9 mL of base added.

$$K_{a,1a} = [H^+]\,[HIn^-] \,/\, [H_2In] \quad (14)$$

$$HIn^- \rightleftharpoons H^+ + In^{2-} \quad (R1b)$$

$$K_{a,1b} = [H^+]\,[In^{2-}] \,/\, [HIn^-] \quad (15)$$

The pK_a that is commonly associated with phenolphthalein at standard temperature is 9.7 [38], which is approximately the value of p$K_{a,1b}$. To use this value and to treat the equilibrium as a single proton dissociation is to assume that all of the phenolphthalein in solution exists as the mono-anion prior to the color change. This is the common approximation and we have calculated the [In^{2-}] values in this manner (Fig. 4, grey squares). However, to more accurately describe the concentration of the colored species In^{2-}, the equilibrium between H_2In and HIn^- must not be neglected. It is clear that the values of p$K_{a,1a}$ and p$K_{a,1b}$ are similar and the dissociations are difficult to separate from each other. Still, one spectrophotometric study reported the values of p$K_{a,1a}$ = 9.05 and p$K_{a,1b}$ = 9.5 [39]. The overall reaction, the double-dissociation given in R1, would then have a pK_{eq} of 18.55. Using the mass balance equation, Eq. (16), and the equilibrium constant expressions, the concentration of the chromophore In^{2-} can be written as Eq. (17) (Fig. 4, grey triangles).

$$[H_2In]_0 = [H_2In] + [HIn^-] + [In^{2-}] \quad (16)$$

$$[In^{2-}] = \frac{K_{eq}[H_2In]_0}{K_{eq} + K_{a,1a}[H^+] + [H^+]^2} \quad (17)$$

The top panel of Fig. 4 shows that the curvature and the inflection point of the vector projection data appear to be in good agreement with the chromophore concentrations calculated by both the single- and double-dissociation methods. The bottom plot in Fig. 4 shows similar

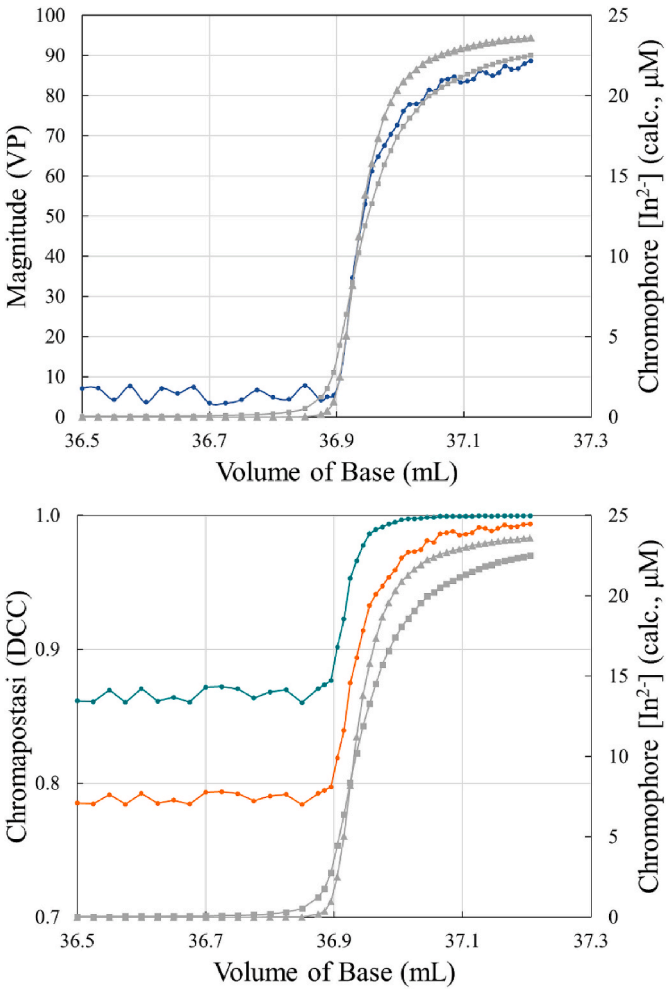

Fig. 4. The top and bottom panels show the results of the vector projection method (dark blue) and the DCC_0 (dark teal) and DCC_{ED} (orange) methods, respectively, as a function of the volume of base added. In both panels, the secondary axis is employed to show the calculated concentration of the colored analyte (grey). Concentrations of the colored analyte were computed in two ways: via single-dissociation approximation pK_a = 9.5 (squares); via the double-dissociation pK_{eq} = 18.55 (triangles).

agreement for the computed DCC_0 and DCC_{ED} values. However, the double-dissociation method is clearly superior because Fig. 5 shows that a good linear correlation of the chromapostasi values as a function of chromophore concentration can only be achieved with the double-dissociation method.

In analogy to Figs. 2 and 5 shows the correlations between the video analysis based chromapostasi values and the calculated chromophore concentration [In^{2-}]. The plot range starts at the emergence of color (36.905 mL of NaOH added). For all three methods, the single dissociation approximation (squares) does not provide a satisfactory linear correlation in any range, and no linear regression line is shown. On the other hand, there is a strong linear correlation between the VPM values (dark blue, primary axis) and the calculated chromophore concentration [In^{2-}] by the double dissociation method (triangles). The DCC_{ED} data (orange, secondary axis) also show very strong linear correlation with the calculated [In^{2-}] and in fact, the linear fit is slightly better than for the VP data. The DCC_0 method fares far worse and the regression line is a very poor fit of the data.

Our results suggest that the VP method and the DCC_{ED} method will be approximately equivalent if the trace in RGB color space closely approximates a straight line. For the phenolphthalein titration, the $R_{s,i}$, $G_{s,i}$, and $B_{s,i}$ values trace out a straight line in color space with increasing

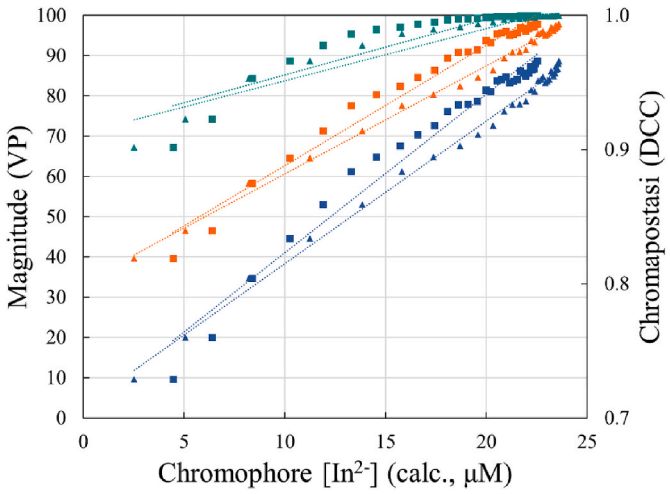

Fig. 5. Chromapostasi values as a function of the chromophore concentration. Comparison of the vector projection method (dark blue, primary axis) and the DCC_0 (dark teal) and DCC_{ED} (orange) methods (secondary axis). Chromophore concentration computed in two ways: via single-dissociation approximation $pK_a = 9.5$ (squares); using the double-dissociation $pK_{eq} = 18.55$ (triangles). R^2 values for single dissociation approximation are 0.9701 (VP), 0.9726 (DCC_{ED}), and 0.8155 (DCC_0) and for the double-dissociation are 0.9953 (VP), 0.9959 (DCC_{ED}), and 0.9178 (DCC_0).

$[In^{2-}]$ (Fig. 3). This is in sharp contrast to the case study of the green dye solution, where the trace in color space (Fig. 1) deviated greatly from linearity. It is this linearity in RGB color space in the region of interest that allows for a judgment of the applicability of the DCC method. The best one can hope for is that the DCC reference point is at the maximum of the region of linearity and in such a case, the DCC method will yield approximately equivalent results.

3.3. Concentration of the Ce^{4+} catalyst in the Belousov-Zhabotinsky oscillating reaction

3.3.1. Total concentration of the Ce^{4+} catalyst

Our genuine interest is with BZ oscillating reactions. In the spirit of the dye analysis, it was our intent to perform video and UV–Vis spectrometric analyses on the same system simultaneously. Another approach, in the spirit of the titration study, would involve the performance of the video analysis in conjunction with the solution of the kinetic equations governing the reaction. We thought that both approaches would provide an independent evaluation of the concentration dependence of the video analyses.

The collection of the UV–Vis data presented several obstacles for the BZ reaction. At first, we attempted to use the same fiber optic dip probe as in the dye experiment. However, CO_2 bubbles produced by the BZ reaction adhere to the surface of the probe, including the surface of the mirror, rendering unreliable readings. Because the oscillation is rapid, removing an aliquot from the bulk solution and measuring its spectrum in a standard cuvette was not feasible for real-time measurements. A flow cell attachment was also considered, but complications arising because of differences between the flow cell and the bulk solution would disrupt any comparison between the UV–Vis spectroscopic and the video analyses. Ultimately, the collection of UV–Vis measurements had to be abandoned.

The mechanism and kinetic rate constants of the BZR have been discussed in the literature for some time [20,21]. Simulations of the kinetic equations to afford real-time concentration data have been developed with some success for the Fe-catalyzed BZ reaction [28], but we have been unable to produce reliable simulations for the Ce-catalyzed reaction over a wide range of reaction conditions using the published rate constants for the Ce^{3+} oxidation and Ce^{4+} reduction processes. Thus, we also cannot compare the results of our video analysis to theoretical concentrations of the $[Ce^{4+}]$ analyte.

Reaction systems with these kinds of complicating factors are exactly the reason why video colorimetry methods are not just desirable but an essential tool. Moreover, we did establish for a series of solutions with various Ce(IV) concentrations in the range pertinent to the BZR that the trace of the single chromophore in color space is linear (*vide infra*).

The initial concentrations of the reagents in the BZ reaction studied were: $KBrO_3$ 74.4 mM; $H_2C(COOH)_2$ 100.5 mM; KBr 19.2 mM; H_2SO_4 0.882 M; $(NH_4)_2Ce(SO_4)_4{\cdot}2\,H_2O$ 4.4 mM and the volume of solution was 300 mL [40]. The video of the BZ reaction was recorded for approximately 58 min or 3500 s. The video data was split into images at a frame rate of 10 images per second, which allows for easy conversion from the image domain to the time domain. The first few minutes of the video show the mixing of the reagents and the induction periods of the BZR. To avoid any leftover induction effects, our analysis begins a few moments before the second oscillation (at 500 s) and continues until the end of the video, approximately 3000 s later. The oscillation pattern remained steady over the entire duration of the video.

The individual R_s, G_s, and B_s values were plotted as a function of time in Fig. 6 for the full time range. The primary change in the color space with each oscillation is a drastic drop in the intensity of the blue channel, which is expected for the increase of the yellow color of the solution with increasing Ce^{4+} concentration. Importantly, none of the color intensities drop below 80 and, as we have shown, this suggests that the chromapostasi values are well within the region that allows for linear correlations with concentration.

Because of the large number of data points, both the VP and the DCC analyses benefit slightly from a smoothing treatment to reduce noise. Data was smoothed by taking a moving average of the magnitude for twenty-one points, the point at time t and its ten nearest neighbors in both directions on the t axis, for a full range of $t \pm 1$ s.

The direct result of the vector projection method, the chromapostasi values, are plotted on the primary axis in the top panel of Fig. 7 and the respective results of the DCC methods are plotted on the secondary axis. For the VP method, the blank image was chosen from a small set of images in the video which occurred after the bromine-containing species had been mixed, but before any cerium was added to the reaction mixture. It is clear that the period time of the reaction is well established by all three methods and averages to about 182 s, although the oscillations do tend to speed up with time.

It is an important observation that VP magnitude drops to almost zero in each cycle, suggesting that the reduction of Ce^{4+} is virtually complete in each cycle. Some noise can be seen in many of the cycles

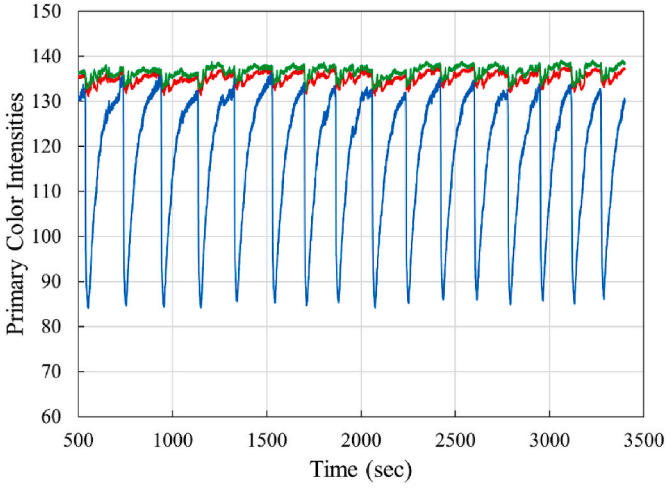

Fig. 6. R_s, G_s, and B_s values for the Ce-catalyzed BZ reaction plotted individually for the full time range.

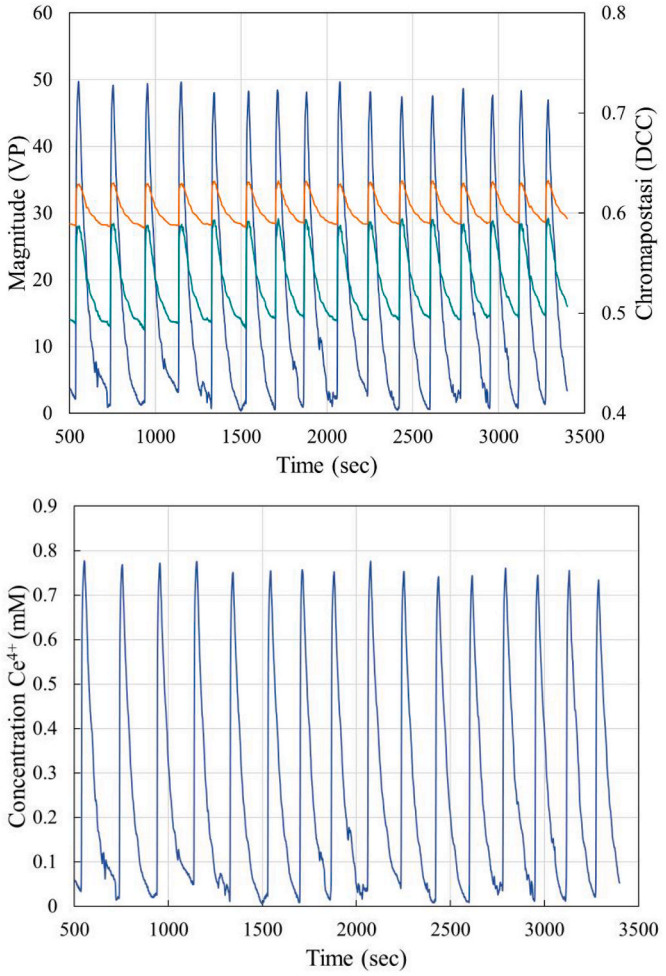

Fig. 7. Top: VP and DCC data for the Ce-catalyzed BZ reaction. The vector projection results (dark blue) are plotted on the primary axis and the results using the DCC_0 (dark teal) and DCC_{ED} (orange) approaches are plotted on the secondary axis. Bottom: Concentration of Ce^{4+} in the BZ reaction as determined by the VP analysis using a 0.6 mM Ce^{4+} standard solution.

when the VP magnitudes are near zero, but this phenomenon is of no concern because the solution is hardly colored in those places. As a consequence of the definition of the DCC values, the chromapostasi parameter related to the Ce^{4+} concentrations remains nonzero, even in the absence of Ce^{4+}. Fig. 7 shows that the lowest DCC_0 and DCC_{ED} values are 0.484 and 0.585, respectively.

If the chromapostasi values derived from the VP method are directly proportional to $[Ce^{4+}]$, then the conversion to the concentration domain requires only one standard solution. A standard solution of Ce^{4+} (0.59 mM) was prepared by dissolving 0.111 g of $(NH_4)_2Ce(SO_4)_4{\cdot}2\ H_2O$ in 300 mL of 1 M sulfuric acid solution. Then, by application of Eq. (10), the Ce^{4+} concentration was determined as a function of time and is shown in the bottom panel of in Fig. 7.

The maximum Ce^{4+} concentration reached in any cycle was approximately 0.77 mM, and hence, a maximum of 14.9% of the cerium in the solution is oxidized. This is compatible with early experimental determinations of the $[Ce^{4+}]/[Ce^{3+}]$ ratio determined by potentiometric methods [20]. The lack of a suitable standard in the DCC dataset makes concentration determinations impossible without reference to the VP data or some other independent method.

3.3.2. Tracing BZ reaction cycles in RGB color space

There was every reason to expect an essentially linear trace in RGB color space for the color associated with the variable $[Ce^{4+}]$ in the course of the BZ reaction. We did know that the respective trace for a series of Ce(IV) salt solutions was essentially linear (Fig. 8, left). To generate the plot of Fig. 8, a stock cerium solution (45.7 mM) was made by dissolving 0.868 g of $(NH_4)_2Ce(SO_4)_4{\cdot}2\ H_2O$ in 30 mL of water. This stock solution was added in 200 μL aliquots to 300 mL of 0.88 M H_2SO_4 and a picture was taken after each addition. The green points in Fig. 8 (left) fall within the range of the Ce^{4+} concentrations of the BZR and the purple points indicate higher cerium(IV) concentrations. As can be seen, the cerium salt series is essentially linear in color space and correlates linearly with $[Ce^{4+}]$. Therefore, we were confident to assume that the VP method would accurately describe the total cerium(IV) concentration in the BZ reaction.

In the right panel of Fig. 8, the smoothed color space trace is shown for a single oscillation of the BZ reaction. Much to our surprise, the color space trace of the BZR cycle was nothing like a simple line. Moreover, the reduction did not re-trace the path of the oxidation causing a well-defined hysteresis loop. Blue points indicate the oxidation phase of the cycle and red points show the reduction phase. During the oxidation phase, the $[Ce^{4+}]$ grows quickly and the growing intensity of the yellow color of the solution is associated with an almost linear color space trace. In the late stages of the oxidation and for the entire duration of the reduction phase, the trace deviates from linearity in a pronounced and intractable fashion. We argue that this feature is real. To demonstrate the reality of an unexpected feature, one needs to establish reproducibility and an oscillating reaction is the perfect system in that regard because, in a sense, every cycle is a reproduction with essentially the same initial conditions.

To demonstrate the reality of the observed hysteresis and its shape-stability, color space plots were generated for several individual periods of the BZ reaction (Fig. 9) and the different colors simply reflect different cycles. Two perspectives are shown of the overlay of these

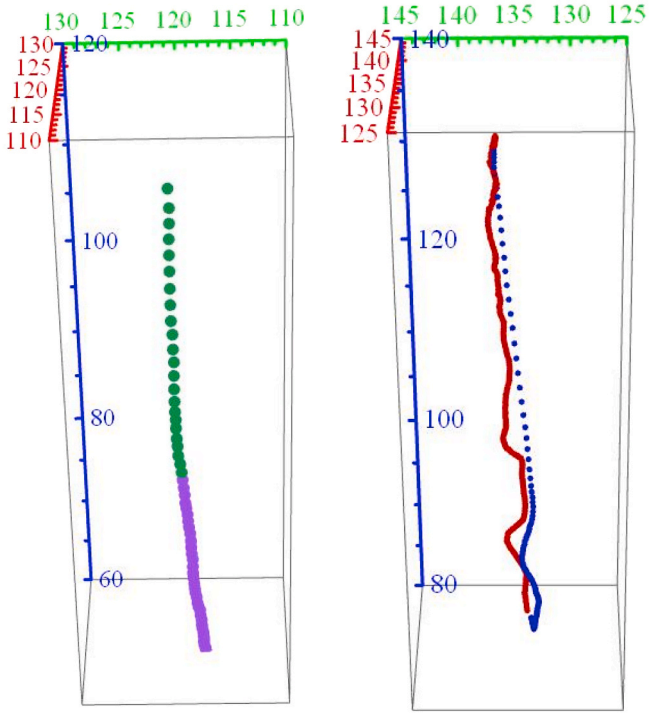

Fig. 8. Each cycle of the BZ reaction features a color change from colorless (Ce^{3+}) to yellow (Ce^{4+}). On the left, the color data are plotted in color space for a series of solutions with various concentrations of a cerium(IV) salt and using false colors to indicate $[Ce^{4+}]$ within the range of the BZ reaction studied (green) and $[Ce^{4+}] > 0.72$ mM (purple). On the right, a similar plot is shown for the color data for one BZR cycle using false colors to indicate the reduction phase (red) and the much shorter oxidation phase (blue).

cycles. Note that the shift of the hysteresis loops in RGB space involves changes of comparable magnitude and comparable direction for the R, G, and B values; shifts of this type are commonly associated with minor lighting fluctuations. Most importantly, the fact that very similar shapes are traced out by all cycles indicates that the fluctuations in color space are not due to noise, but have real, chemical significance.

Typical discussions of the Ce-catalyzed Belousov-Zhabotinsky reaction merely refer to the oscillation between "Ce^{3+}" and "Ce^{4+}", as we have done above. In reality however, both cerium ions are present as complexes in solution. Under BZR conditions, it is most likely that sulfate species occupy the coordination sphere [41–44] and the crystallographic record includes examples of such complexes [45–47]. The color of Ce(IV) complexes is known to be sensitive to the nature of ligation and large shifts in the emitted light have been documented [48]. During the fast oxidation of the predominant Ce^{3+} species, the linearity of the RGB trace of the generated Ce^{4+} species suggests minimal changes in the ligation. It is only in the later stages of the oxidation phase that the initially-formed Ce^{4+} complexes optimize their coordination sphere and this may include some ligand exchanges/additions. Reduction of the cerium(IV) complexes requires the approach of bromomalonic acid, the reducing agent, and its integration into the primary coordination sphere. The primary product of bromomalonic acid oxidation is mesoxalic acid [22,49], itself a powerful tridentate ligand. Eventually, the ligand sphere of the freshly-reduced cerium ion will lose the organic ligands

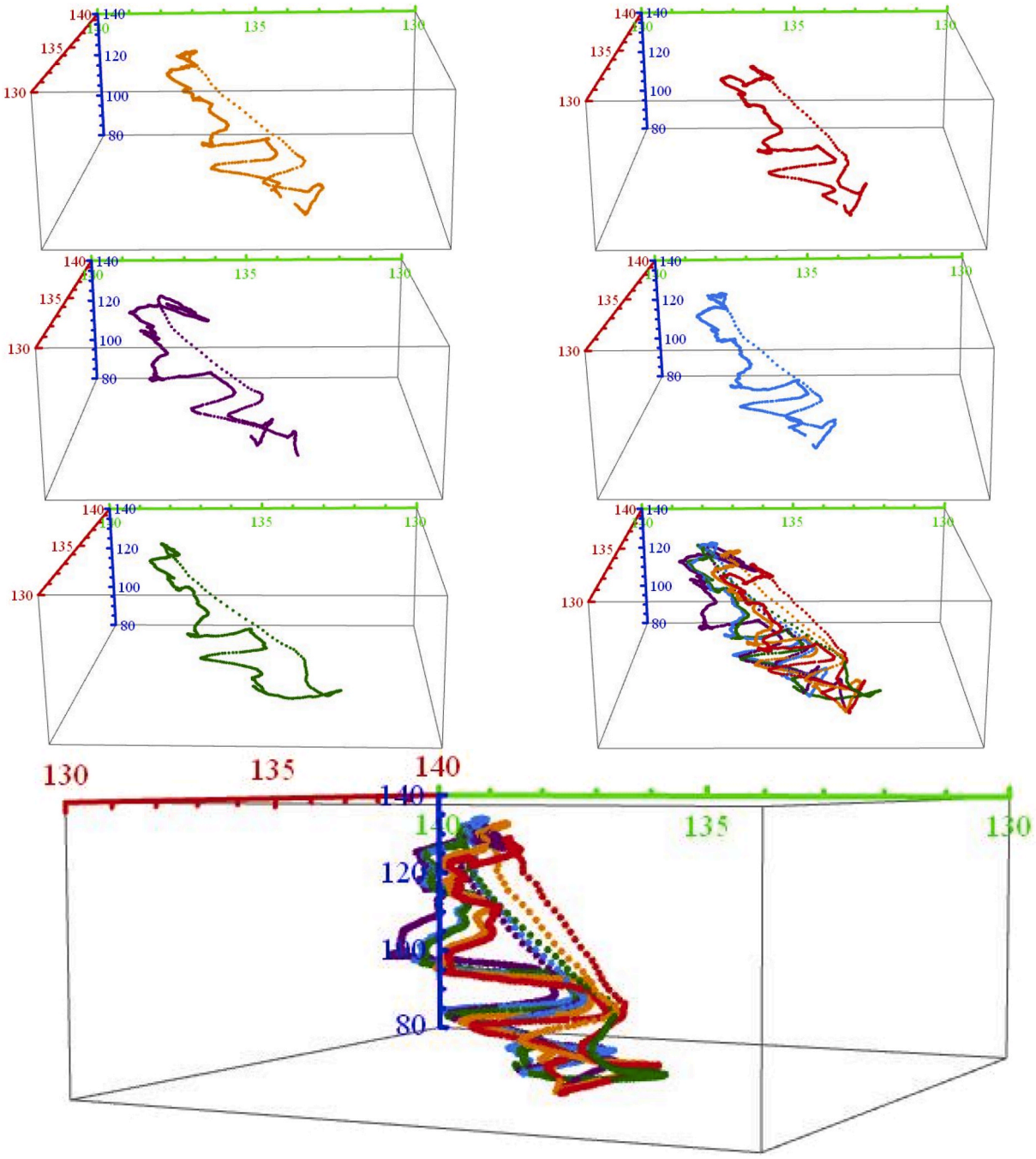

Fig. 9. Hysteresis loops of the [Ce^{4+}] colorimetric analysis in color space for sequential oxidation/reduction cycles of the cerium-catalyzed BZ reaction. False colors are used for different cycles; cycles 3–7 are displayed left-to-right and top-to-bottom. The overlay of the five cycles shows some migration of the hysteresis loop in RGB space, while maintaining shape-stability.

and return to the dominant cerium(III) sulfate complex. Even a minimalistic consideration must include at least three types of Ce^{4+} complexes with different ligands. Every type of cerium(IV) complex will have its characteristic color and, hence, it should not be surprising that the color trace of this complicated reaction is not linear in RGB space. The BZ reaction clearly involves more than a single chromophore.

The RGB color space analysis provides compelling evidence for the presence of several similar chromophores. *A priori*, the chromophores will have their own slightly different colors and distinct extinction coefficients. In a strict sense, the RGB color space analysis therefore does not provide a perfect concentration measurement in this case. Nevertheless, the concentration curves shown in Fig. 7 still provide the best possible estimate of total [Ce^{4+}] content.

It was our original intent to compare the video analysis to UV–Vis absorbance measurements in order to validate the former by the latter. This approach relies on the assumption of one species being responsible for the UV–Vis absorbance. The color space analysis shows that there are several chromophores and alerts to possible limitations of the colorimetric determination of concentration. The UV–Vis measurement, on the other hand, would not have been able to provide any indication of the presence of multiple chromophores because of low resolution of the instrument.

4. Conclusion

We have developed a colorimetric method, the vector projection (VP) method, to determine the concentration of a single chromophore reliably from video data. It is one of the major advantages of the VP method that this analysis is conceptually intelligible and can be visualized in three-dimensional RGB color space. In particular, by mapping the changes in the primary color intensities in 3D color space, one can determine whether the results of the image analysis will correlate linearly with chromophore concentration. We have shown that the VP data will correlate linearly with chromophore concentration so long as the RGB vectors trace a straight line in color space. Linear traces are more likely for processes associated with color changes that retain significant intensity in all primary color channels.

The VP method and the DCC methods both rely on one reference. The VP method uses a blank solution (measuring background) while the DCC methods use a relatively concentrated solution of the analyte (intense color standard). The VP method is insensitive to the precise choice of standard, while the selection of the DCC standard is non-trivial and a good choice requires prior knowledge of the system. The insights led to the definition of the improved DCC_{ED} method, which is capable of producing results that match the quality obtained by the VP method.

In two proof of concept studies, we compared the performance of the colorimetric methods to independent measurements of concentrations. UV–Vis absorption data provided the independent reference in an analysis of a series of dye solutions of variable concentration. Calculations of the chromophore concentration as a function of pH were employed for the quality assessment of the colorimetric analysis of the titration with phenolphthalein indicator. Both cases provide direct evidence that the VP method allows for the determination of accurate chromophore concentrations if the RGB vectors trace a straight line in color space. The titration experiment showcased excellent agreement between the colorimetrically-determined and the computed chromophore concentrations and demonstrated in a compelling fashion that the VP analysis is perfectly able to reliably capture fast color changes which follow a complicated kinetics.

The application of the colorimetric methods to the video-based analysis to a Ce-catalyzed BZ oscillating reaction provided an impressive demonstration of their powerful capabilities to study fast reactions with complicated kinetics. The colorimetric methods are easy to apply and their temporal resolution far exceeds that of visible spectroscopy instrumentation. The VP and the DCC methods all produce highly accurate timing information. The VP method is the method of choice to measure single-chromophore concentrations over time and the VP method produces the best possible estimates of total Ce^{4+} content. Shape-stable hysteresis loops in RGB space reveal small but systematic color changes within a BZR cycle and especially in the course of the reduction phase. The hysteresis loops inform about mechanistic complexities that would have been impossible to obtain via standard spectroscopy. The observed hysteresis loops suggest changes in the ligation of the cerium(IV) chromophore and further studies are needed to explore the impact of ligands on the 320 nm absorption of cerium(IV) ions. The observation of hysteresis loops also demonstrates the advantage of three-color analysis as compared to the commonly used single-channel colorimetric methods. Observation of the BZ reaction using just the blue channel would be an obvious choice for single-channel colorimetry. Yet, this choice would preempt the discovery of the rich redox reaction chemistry.

Authorship contribution statement

Joseph Schell: Investigation – experimental design & measurements, Colorimetry – concept design & software development, Visualization, Mentoring, Contextualization, Interpretation, Writing - original draft & editing. Sara McCauley: Investigation – experimentation & data collection, Illustration, Visualization, Contextualization, Writing - contributing. Rainer Glaser: Funding acquisition, Supervision, Mentoring, Conceptualization, Interpretation, Writing - review & editing.

Declaration of competing interest

The authors have no competing interest.

Acknowledgments

The authors thank Dr. Carmen Chicone, Marco Downing, and Ethan Zars for their contributions to the development of DCC methods and their application to video-based kinetic studies. This research was supported by the Missouri University of Science and Technology and, in part, by NSF grant #1665487. SM gratefully acknowledges support by FYRE and OURE scholarships.

Appendix A. Supplementary data

Supplementary data to this article can be found online at https://doi.org/10.1016/j.talanta.2020.121303.

References

[1] F. Wang, Y. Lu, J. Yang, Y. Chen, W. Jing, L. He, Y. Liu, A smartphone readable colorimetric sensing platform for rapid multiple protein detection, Analyst 142 (2017) 3177–3182.
[2] S. Dutta, Point of care sensing and biosensing using ambient light sensor of smartphone: critical review, TrAC Trends Anal. Chem. (Reference Ed.) 110 (2019) 393–400.
[3] M. Shariati-Rad, F. Fattahi, A simple equipment and colorimetric method for determination of chloroform in water, Anal. Chim. Acta 1100 (2020) 208–214.
[4] E.N. Gaiao, V.L. Martins, W.S. Lyra, L.F. Almeida, E.C. Silva, M.C.U. Araújo, Digital image based titrations, Anal. Chim. Acta 570 (2006) 283–290.
[5] W.S. Lyra, V. Santos, A. Dionízio, V. Martins, L. Almeida, E.N. Gaiao, P. Diniz, E. Silva, M. Araújo, Digital image-based flame emission spectrometry, Talanta 77 (2009) 1584–1589.
[6] L.F. Capitán-Vallvey, N. López-Ruiz, A. Martínez-Olmos, M.M. Erenas, A.J. Palma, Recent developments in computer vision-based analytical chemistry: a tutorial review, Anal. Chim. Acta 899 (2015) 23–56.
[7] N. Maleki, A. Safavi, F. Sedaghatpour, Single-step calibration, prediction and real samples data acquisition for artificial neural network using a CCD camera, Talanta 64 (2004) 830–835.
[8] A. Choodum, P. Kanatharana, W. Wongniramaikul, N. NicDaeid, Rapid quantitative colourimetric tests for trinitrotoluene (TNT) in soil, Forensic Sci. Int. 222 (2012) 340–345.
[9] L.P. dos Santos Benedetti, V.B. dos Santos, T.A. Silva, E.B. Filho, V.L. Martins, O. Fatibello-Filho, A digital image-based method employing a spot-test for quantification of ethanol in drinks, Anal. Methods 7 (2015) 4138–4144.

[10] A. Rico-Yuste, V. González-Vallejo, E. Benito-Peña, T. de las Casas Engel, G. Orellana, M.C. Moreno-Bondi, Furfural determination with disposable polymer films and smartphone-based colorimetry for beer freshness assessment, Anal. Chem. 88 (2016) 3959–3966.

[11] A. Choodum, K. Parabun, N. Klawach, N. NicDaeid, P. Kanatharana, W. Wongniramaikul, Real time quantitative colourimetrice test for methamphetamine detection using digital and mobile phone technology, Forensic Sci. Int. 235 (2014) 8–13.

[12] D. Merli, A. Profumo, S. Tinivella, S. Protti, From smart drugs to smartphone: a colorimetric spot test for the analysis of the synthetic cannabinoid AB-001, Forensic Chem 14 (2019) 100167.

[13] A. Lopez-Molinero, V.T. Cubero, R.D. Irigoyen, D.S. Piazuelo, Feasibility of digital image colorimetry—application for water calcium hardness determination, Talanta 103 (2013) 236–244.

[14] M.L. Firdaus, W. Alwi, F. Trinoveldi, I. Rahayu, L. Rahmidar, K. Warsito, Determination of chromium and iron using digital image-based colorimetry, Procedia Environ. Sci. 20 (2014) 298–304.

[15] A. Martin, F. Portaels, J.C. Palomino, Colorimetric redox-indicator methods for the rapid detection of multidrug resistance in mycobacterium tuberculosis: a systematic review and meta-analysis, J. Antimicrob. Chemother. 59 (2007) 175–183.

[16] E. Vega-Avila, M.K. Pugsley, An overview of colorimetric assay methods used to assess survival or proliferation of mammalian cells, Proc. West. Pharmacol. Soc. 54 (2011) 10–14.

[17] V.V. Apyari, S.G. Dmitrienko, Y.A. Zolotov, Analytical possibilities of digital colorimetry: determination of nitrite using polyurethane foam, Moscow Univ. Chem. Bull. 66 (2011) 32–37.

[18] W. Li, R. Zhang, H. Wang, W. Jiang, L. Wang, H. Li, T. Wu, Y. Du, Digital image colorimetry coupled with a multichannel membrane filtration-enrichment technique to detect low concentration dyes, Anal. Methods 8 (2016) 2888–2894.

[19] W. Dong, A.P.S. Selvadurai, Image processing technique for determining the concentration of a chemical in a fluid-saturated porous medium, Geotech. Test J. 29 (2006) 385–391.

[20] R.J. Field, E. Körös, R.M. Noyes, Oscillations in the chemical systems II. Thorough analysis of temporal oscillation in the bromate-cerium-malonic acid system, J. Am. Chem. Soc. 94 (1972) 8649–8664.

[21] L. Hegedüs, M. Wittmann, Z. Noszticzius, S. Yan, A. Sirimungkala, H.-D. Försterling, R.J. Field, HPLC analysis of complete BZ systems. Evolution of the chemical composition in cerium and ferroin catalysed batch oscillators: experiments and model calculations, Faraday Discuss 120 (2001) 21–38.

[22] A.F. Taylor, Mechanism and phenomenology of an oscillating chemical reaction, Progr. React. Kinet. Mech. 27 (2002) 247–325.

[23] Z. Nagy-Ungvarai, S.C. Müller, J.J. Tyson, B. Hess, Experimental study of the chemical waves in the Ce-catalyzed Belousov-Zhabotinskii reaction. 2. Concentration profiles, J. Phys. Chem. 93 (1989) 2760–2764.

[24] S.C. Müller, T. Plesser, B. Hess, The structure of the core of the spiral wave in the Belousov-Zhabotinskii reaction, Science 230 (1985) 661–663.

[25] A. Pagola, C. Vidal, Wave profile and speed near the core of a target pattern in the Belousov-Zhabotinsky reaction, J. Phys. Chem. 91 (1987) 501–503.

[26] R. Glaser, M. Jost, Disproportionation of bromous acid HOBrO by direct O-transfer and via anhydrides $O(BrO)_2$ and $BrO–BrO_2$. An ab initio study of the mechanism of a key step of the Belousov–Zhabotinsky oscillating reaction, J. Phys. Chem. 116 (2012) 8352–8365.

[27] R. Glaser, Why the acidity of bromic acid really matters for kinetic models of Belousov-Zhabotinsky oscillating chemical reactions, J. Therm. Catal. 4 (2013) e115.

[28] E. Zars, R. Glaser, M. Downing, C. Chicone, Measurements and simulations of the acidity dependence of the kinetics of the iron-catalyzed Belousov-Zhabotinsky reaction. Proton-catalysis in the electron transfer reaction involving the $[Fe(phen)_3]^{3+}$ species, J. Phys. Chem. 122 (2018) 6183–6195.

[29] R.E. Glaser, M. Downing, E. Zars, J. Schell, C. Chicone, Video-based kinetic analysis of period variations and oscillation patterns in the Ce/Fe-catalyzed four-color Belousov-Zhabotinsky oscillating reaction (Chapter 15) in, in: Marcy H. Towns, Kinsey Bain, Jon-Marc G. Rodriguez (Eds.), It's Just Math: Research on Students' Understanding of Chemistry and Mathematics, ACS Symposium Series 1316, American Chemical Society, Washington, DC, 2019, pp. 251–270.

[30] B. Coleman, C. Coarsey, M.A. Kabir, W. Asghar, Point-of-care colorimetric analysis through smartphone video, Sensor. Actuator. B Chem. 282 (2019) 225–231.

[31] Aoao photo, <http://www.aoaophoto.com> (accessed 03/18/2020).

[32] Aoao Video to Picture Converter, < https://www.aoaophoto.com/video-to-picture-converter/video-to-picture.htm > (accessed 03/18/2020).

[33] D.C. Harris, C.A. Lucy, Fundamentals of Spectroscopy, in: Chapter 17 in Quantitative Chemical Analysis, W.H. Freeman & Company, New York, 2010.

[34] Wolfram Research, Inc., Mathematica, 2019. Version 12.0.0.0, Champaign, IL, https://reference.wolfram.com/language/ref/ImageTake.html. accessed 03/18/2020.

[35] R.E. Glaser, M.A. Delarosa, A.O. Salau, C. Chicone, Dynamical approach to multiequilibria problems for mixtures of acids and their conjugated bases, J Chem. Educ. 91 (2014) 1009–1016.

[36] E. Zars, J. Schell, M.A. Delarosa, C. Chicone, R. Glaser, Dynamical approach to multi-equilibria problems considering the Debye–Hückel theory of electrolyte solutions: concentration quotients as a function of ionic strength, J. Solut. Chem. 46 (2017) 643–662.

[37] J. Schell, E. Zars, C. Chicone, R. Glaser, Simultaneous determination of all species concentrations in multiequilibria for aqueous solutions of dihydrogen phosphate considering Debye–Hückel theory, J. Chem. Eng. Data 63 (2018) 2151–2161.

[38] J.R. Rumble, D.R. Lide, T.J. Bruno, Dissociation constants of organic acids and bases, in: Section 5 in: CRC Handbook of Chemistry and Physics, 100th ed., 2019, p. 41. Boca Raton, FL.

[39] Z. Tamura, S. Abe, K. Ito, M. Maeda, Spectrophotometric analysis of the relationship between dissociation and coloration, and of the structural formulas of phenolphthalein in aqueous solution, Anal. Sci. 12 (1996) 927–930.

[40] B.Z. Shakhashiri, Chemical Demonstrations. A Handbook for Teachers of Chemistry, vol. 2, University of Wisconsin Press, Madison, WI, 1989.

[41] S.B. Hanna, R.R. Kessler, A. Merbach, S. Ruzicka, Planning a kinetic and mechanistic study with cerium(IV), J. Chem. Educ. 53 (1976) 524–527.

[42] S.B. Hanna, R.K. Hessley, L.M. Nicholson, Kinetic identification of the reactive cerium(IV) species in the oxidation of the methyliminodiacetic acid (MIDA) in acidic sulfate media, Inorg. Chim. Acta. 25 (1977) L7–L8.

[43] T.J. Hardwick, E. Robertson, Association of ceric ions with sulphate (a spectral study), Can. J. Chem. 29 (1951) 828–837.

[44] J.C. Sullivan, R.C. Thompson, Kinetic study of the cerium(IV)-bromous acid reaction in sulfate solution. Implications for the Belousov-Zhabotinskii oscillating reaction, Inorg. Chem. 18 (1979) 2375–2379.

[45] B.M. Gatehouse, A. Pring, The crystal structure of hydrogen cerium(III) sulfate hydrate, $[H_3O][Ce(SO_4)_2]·H_2O$, J. Solid State Chem. 38 (1981) 116–120.

[46] O. Lindgren, The crystal structure of cerium(IV) sulfate tetrahydrate, $Ce(SO_4)_2·4H_2O$, Acta Chem. Scand., Ser. A 31 (1977) 453–456.

[47] O. Lindgren, The crystal structure of sodium cerium(III) sulfate hydrate, $NaCe(SO_4)_2·H_2O$, Acta Chem. Scand., Ser. A 31 (1977) 591–594.

[48] D. Werner, G.B. Deacon, P.C. Junk, R. Anwander, Cerium(III/IV) formamidinate chemistry, and a stable cerium(IV) diolate, Chem. Eur J. 20 (2014) 4426–4438.

[49] L. Hegedüs, H.-D. Försterling, M. Wittman, Z. Noszticzius, Ce^{4+}-malonic acid reaction in the presence of O_2. Reaction channels leading to tartronic and oxalic acid intermediates, J. Phys. Chem. 104 (2000) 9914–9920.